Aalborg Universitet

Passivity-Based Harmonic Stability Analysis of an Offshore Wind Farm Connected to a MMC-HVDC

Wu, Heng; Wang, Xiongfei; Kocewiak, ukasz Hubert; Hjerrild, Jesper; Kazem, Mohammad

Passivity-Based Harmonic Stability Analysis of an Offshore Wind Farm Connected to a MMC-HVDC

Heng Wu and Xiongfei Wang
Dept. of Energy Technology
Aalborg University
Aalborg, Denmark
hew, xwa@et.aau.dk

Łukasz H.Kocewiak, Jesper Hjerrild and Mohammad Kazem Bakhshizadeh
Wind Power, Ørsted
Fredericia, Denmark
lukko, jeshj, modow@ orsted.dk

Abstract---**Large offshore wind farms (OWFs) connected to a modular multilevel converter (MMC) based high-voltage direct current (HVDC) transmission system may experience electrical resonance in a wide frequency range. The frequency-domain passivity theory offers an effective method for the stability assessment. This paper performs a systematic passivity-based stability analysis of an OWF connected to a MMC-HVDC, where the controller parametric effect on system passivity is thoroughly investigated, and guidelines for minimizing the non-passive region of OWFs and MMC-HVDC by optimizing controller parameters is provided. It is found out that much better stability robustness of the system can be achieved if the central frequency of the notch filter used in the OWF control is tuned lower than the network resonance frequency. Time-domain simulations are given to verify the theoretical analysis.**

Index Terms—**Offshore wind farm, modular multilevel converter, small-signal stability, passivity.**

I. INTRODUCTION

Large offshore wind farms (OWFs) connected to a modular multilevel converter (MMC) based high-voltage direct current (HVDC) transmission system may experience electrical resonance in a wide frequency range, due to the dynamic interaction between different power electronic converters and passive networks [1]-[2]. A number of incidents have been reported from the commissioned projects with oscillations between OWF and MMC-HVDC [3]. Therefore, stability analysis methods for the overall system is urgently needed.

The impedance-based stability criterion [4], which is derived based on the Nyquist stability criterion, is a powerful tool for the stability assessment of a simple electrical system. Yet, the complexity of the stability analysis increases significantly with a large system including an OWF with a MMC-HVDC, where it is required to carry out the stability analysis for different operating scenarios (energizing cables/transformers, connection/disconnection cables/transformers/wind turbines, etc). Therefore, performing the stability analysis case by case is time-consuming, and it is also difficult to identify the worst case in terms of stability.

On the other hand, the frequency-domain passivity theory offers an effective method for stability assessment [5]-[6]. Suppose that all power electronic converters, have a passive behavior, i.e., the real part of the input admittance is nonnegative for all frequencies. Then, the system is stable regardless of the change of network topologies, as the network, which consists of cables, transformers, shunt reactors, etc., is passive itself and is always stable. Therefore, there is no need to go through every operating scenario during the stability analysis, which overcomes the disadvantages of the impedance-based stability analysis method.

The passivity based stability analysis of OWFs has been reported in recent literatures [5]-[6], but the passivity analysis of the MMC-HVDC has not drawn much attention. To fill this void, this paper thus performs a systematic passivity based stability analysis of the OWF with MMC-HVDC, where the controller parametric effect on system passivity is thoroughly investigated, and guide lines for minimizing the non-passive region of OWFs and MMC-HVDC by optimizing controller parameters is provided.

Electrical oscillation may appear if the network resonance frequency falls into the frequency range of the non-passive region of the OWF and MMC-HVDC. The typical solution is using a notch filter to attenuate this oscillation, which requires the central frequency of the notch filter to be tuned exactly same as (or at least very close to) the network resonance frequency [7]-[11]. However, the network resonance frequency may change due to the change of system configuration and/or parameter variation, and thus the system robustness cannot be guaranteed. This paper re-investigates the stabilization effect of the notch filter from the passivity perspective, and it is found that much better stability robustness can be achieved if the central frequency of the notch filter is tuned lower than the network resonance frequency. Time-domain simulations are given to verify the theoretical analysis. The outcome of this paper is expected to provide more insight to vendors as well as system operators in terms of passivity enhancement of an OWF with MMC-HVDC.

II. PASSIVITY-BASED HARMONIC STABILITY ANALYSIS

A. System Description

Fig. 1 illustrates the system configuration of two OWFs connected to the MMC-HVDC through step up transformers. For simplicity, each OWF is aggregated as one wind turbine (WT) converter. Fig. 2 shows the equivalent circuit diagram, where the current controlled WT converter is modeled as an ideal current source with its paralleled impedance Z_{WT}, and the voltage controlled MMC is modeled as an ideal voltage source
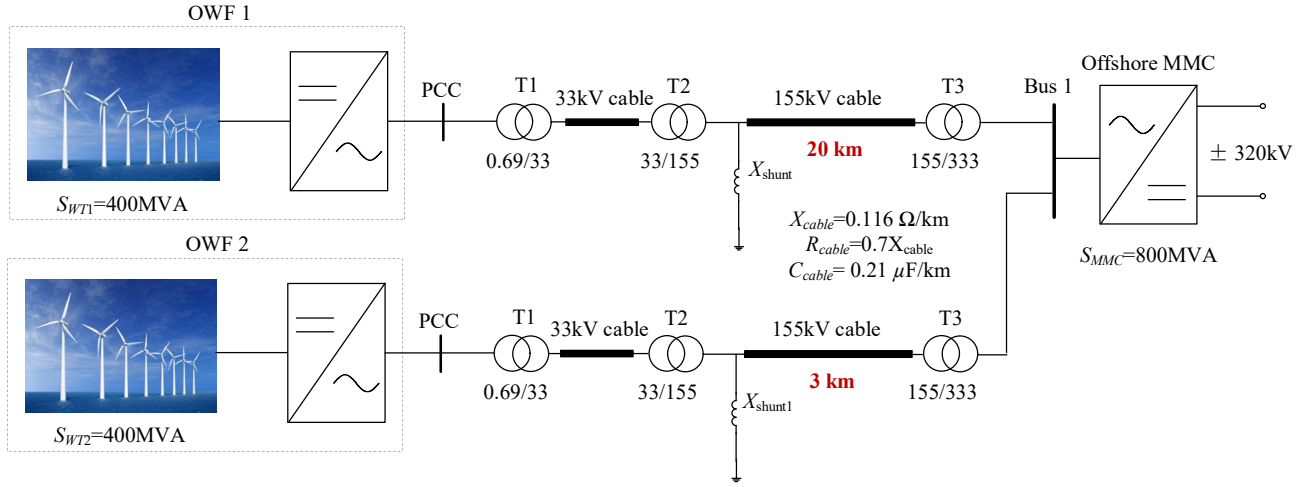
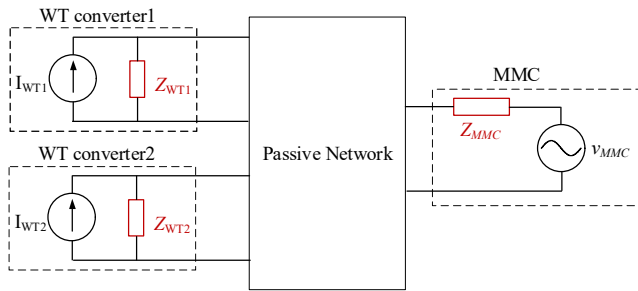Fig. 1. System configuration of the OWFs connected to the MMC-HVDC

Fig. 2. Equivalent circuit diagram of OWFs connected to the MMC-HVDC.

with its series impedance Z_{MMC}. Since the network between the WT converters and the MMC is passive. The system will be stable if Z_{WT} and Z_{MMC} have non-negative real part in the whole frequency range of interest, i.e., Re(Z_{WT})>0 and Re(Z_{MMC})>0.

B. Passivity Analysis of the MMC-HVDC

Fig. 3 shows the circuit and control diagram of the offshore MMC. The output voltage of the MMC is controlled with constant magnitude and frequency. G_{vd} represents the voltage regulator. R_d and G_{HPF} represent the active resistor and high pass filter used in the active damping, respectively. $e^{-sT_{dMMC}}$ represents the total delay introduced by the sampling, control and modulation of the MMC, where T_{dMMC} represents the delay time. The internal dynamics of the MMC can be neglected when deriving its high-frequency output impedance [12], which is given by:

$$Z_{MMC}(s) = \frac{(sL_{arm}+R_{arm})/2 + R_d e^{-sT_{dMMC}} G_{HPF}}{1+V_{dc}G_{vd}e^{-sT_{dMMC}}}. \quad (1)$$

$$G_{vd} = K_{pMMC} + K_{rMMC}\frac{s}{s^2+\omega_0^2}. \quad (2)$$
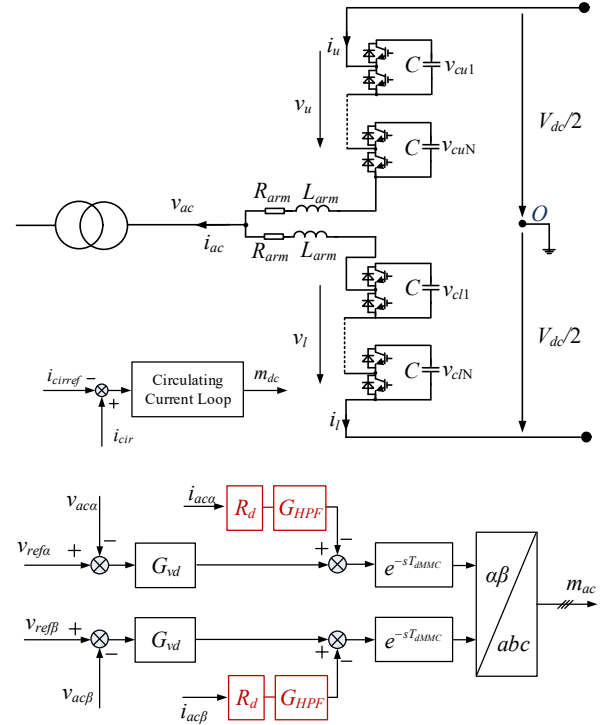
$$G_{HPF} = \frac{s}{s+\omega_{HPF}}. \quad (3)$$

Fig. 3. Circuit and control diagram of the offshore MMC

where K_{pMMC} and K_{rMMC} are the proportional and resonant gain of G_{vd}, respectively, while ω_{HPF} is the cross-over frequency of G_{HPF}.

Note that $R_d e^{-sT_{dMMC}}$ in (1) can be written with its Euler expansion, i.e.,

$$R_d e^{-j\omega T_{dMMC}} = R_d\left[\cos(\omega T_{dMMC}) - j\sin(\omega T_{dMMC})\right]. \quad (4)$$

The critical frequency is defined as $f_{criticalmmc}=1/(4T_{dMMC})$. It is known from (4) that $R_d\cos(\omega T_{dMMC})<0$ if $2\pi f_{criticalmmc}< \omega < 6\pi\ f_{criticalmmc}$, indicating that the active damping actually introduces the negative resistor in that frequency range due to the delay impact, which may lead to the non-passive region of Z_{MMC}.

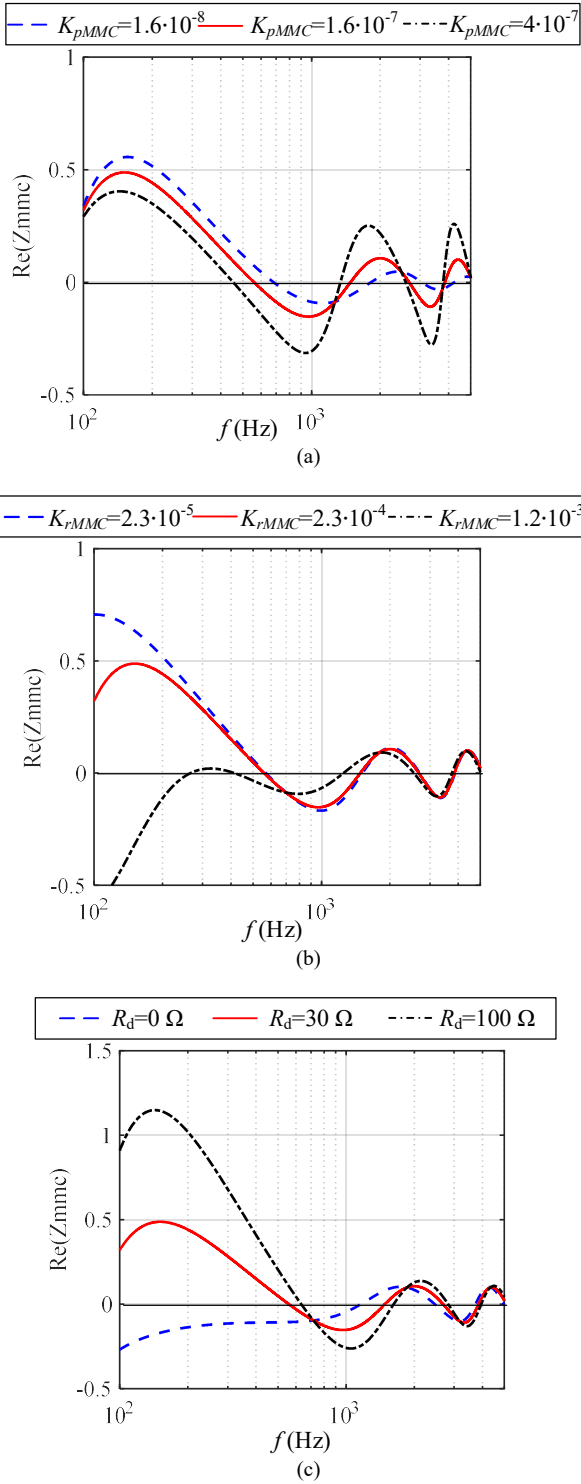Fig. 4 shows the parametric impact on the passivity of the

(a)

(b)

(c)

Fig. 4. Parametric impact on the passivity of the offshore MMC (a) Real part of the output impedance of the MMC with different K_{pWT} values. (b) Real part of the output impedance of the MMC with different K_{rWT} values. (c) Real part of the output impedance of the MMC with different R_d values.

offshore MMC. It is clear that the system designed with fast dynamics, i.e., larger K_{pMMC} and K_{rMMC} values, generally leads to larger negative real part of Z_{MMC} in the high frequency range, as shown in Fig. 4 (a) and (b). Therefore, careful tradeoff between the system stability and dynamic performance is needed during the parameters tuning procedure. As the objective of the resonant part of G_{vd} is merely to mitigate the

steady-state control error, choosing a small K_{rMMC} is recommended from the stability perspective. Moreover, $\mathrm{Re}(Z_{MMC})<0$ in the low frequency range can be observed in Fig. 4 (c) if there is no active damping ($R_d=0$), which highlights the necessity of using the active damping to stabilize the system. On the other hand, although $\mathrm{Re}(Z_{MMC})>0$ in the low frequency range can be guaranteed by using the active damping, too large R_d will also lead to large negative damping in the high frequency range due to the delay impact, as shown in Fig. 4 (c).

C. Passivity Analysis of the Wind Turbine Converter

Fig. 5 shows the circuit and control diagram of the WT converter. The output current of the WT converter is controlled to track its reference value. G_{id} represents the current regulator, and G_{LPF} represents the low pass filter used in the grid voltage feedforward path. $e^{-sT_{dWT}}$ represents the total delay introduced by the sampling, control and modulation of the WT converter, where T_{dWT} represents the delay time. Since the harmonic stability is of concern, the dynamics of the DC voltage loop, reactive power loop and the PLL can be neglected during the impedance modeling procedure. The output impedance of the WT converter is expressed as:

$$Z_{WT}(s) = \frac{sL_f + R_f + V_{dc}G_{id}e^{-sT_{dWT}}}{1 - G_{LPF}e^{-sT_{dWT}}}. \tag{5}$$

$$G_{id}(s) = K_{pWT} + K_{rWT}\frac{s}{s^2 + \omega_0^2}. \tag{6}$$

$$G_{LPF} = \frac{\omega_{LPF}}{(s - j\omega_0) + \omega_{LPF}}. \tag{7}$$

where K_{pWT} and K_{rWT} are the proportional and resonant gain of G_{id}, respectively, while ω_{LPF} is the cross over frequency of G_{LPF}.
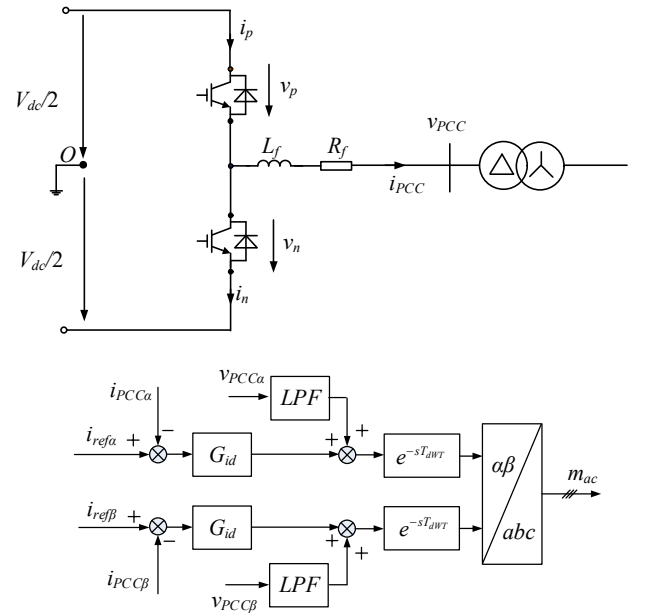

Fig. 5. Circuit and control diagram of the WT converter

Similar to the analysis in Section II-B, $K_{pWT}\cos(\omega T_{dWT})$ in (5) will be smaller than zero if $2\pi f_{critical\mathrm{WT}}< \omega < 6\pi f_{critical\mathrm{WT}}$, where $f_{critical\mathrm{WT}}=1/(4T_{dWT})$, which indicates the proportional
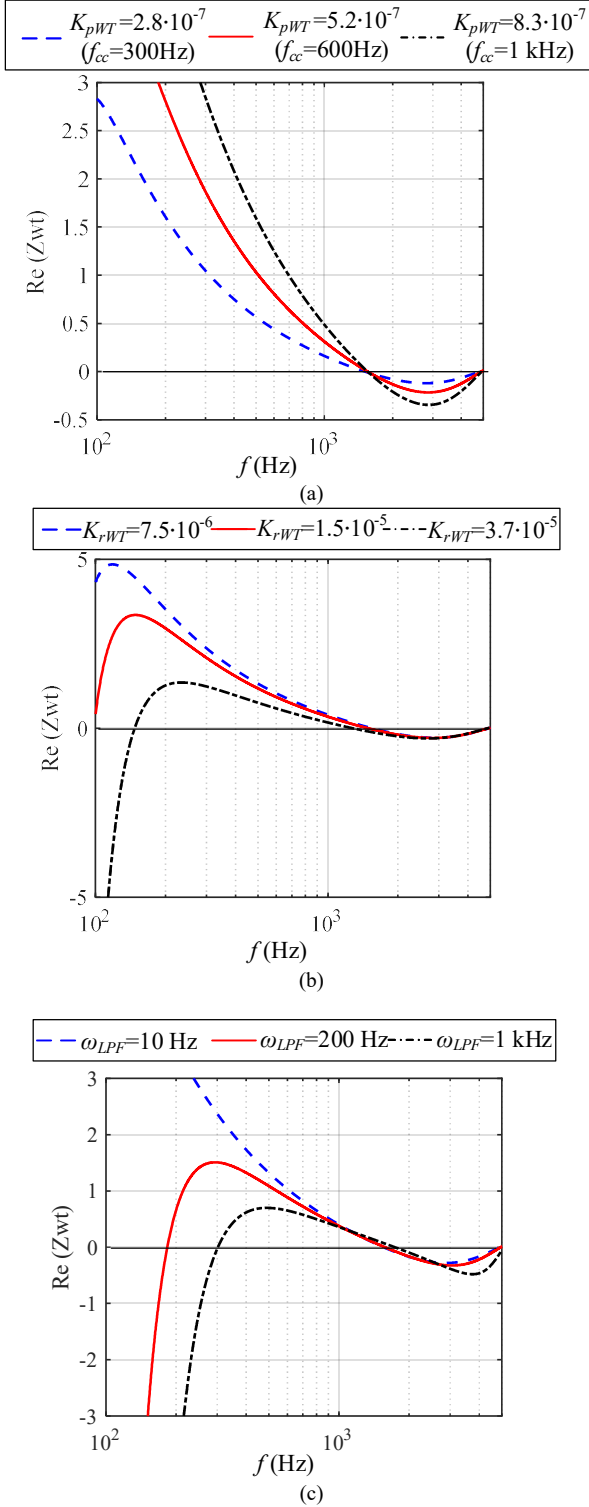

(a)

(b)

(c)

Fig. 6. Parametric impact on the passivity of the WT converter. (a) Real part of the output impedance of the WT converter with different K_{pWT} values. (b) Real part of the output impedance of the WT converter with different K_{rWT} values. (c) Real part of the output impedance of the WT converter with different ω_{LPF} values.

gain in the current regulator introduces the negative resistor in that frequency range due to the delay impact, which may lead to the non-passive region of Z_{WT}.

Fig. 6 shows the parametric impact on the passivity of the WT converter, the conclusion is basically the same with that concluded in Section II-B, i.e., the system designed with fast dynamics (larger K_{pWT}, K_{rWT} and ω_{LPF}.) leads to the larger negative real part of Z_{WT} in the high frequency range, which jeopardizes the system stability, as shown in Figs. 6 (a)-(c).

III. STABILITY ENHANCEMENT METHOD

The notch filter is widely used in the WT converter to mitigate the harmonic oscillation, as shown in Fig. 7, where ω_N represents the central frequency of the notch filter. Different from the existing work [7]-[11], this paper will demonstrate that a more robust system can be achieved by tuning ω_N to be slightly lower than the resonant frequency of the electrical system.

The output impedance of the WT converter with the notch filter is expressed as:

$$Z_{WT}\left(s\right) = \frac{sL_f + R_f + V_{dc}G_{id}e^{-sT_{dWT}}\,G_{notch}}{1-G_{LPF}e^{-sT_{dWT}}}. \qquad (8)$$

where

$$G_{notch}\left(s\right) = \frac{s^2 + \omega_N^2}{s^2 + 2\omega_i s + \omega_N^2}. \qquad (9)$$

Fig. 8 shows the bode diagram of the notch filter, it is clear that the notch filter introduces the phase leading characteristic beyond ω_N, which compensates the phase lagging introduced by the system delay in (5). Therefore, the real part of Z_{WT} is increased after ω_N, which is confirmed in Fig. 9.

From Fig. 9, it is clear that if the electrical resonance with frequency ω_{res} occurs due to the lack of damping, it is better to choose ω_N slightly smaller than ω_{res} for the damping improvement, rather than $\omega_N \approx \omega_{res}$. However, it should be noted that system passivity will be jeopardized by the notch filter in the frequency range lower than ω_N, and thus careful investigation regards the risk of introducing new resonances in this frequency range is needed before implementing the notch filter.
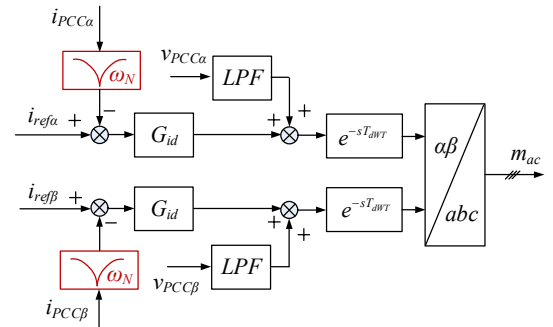

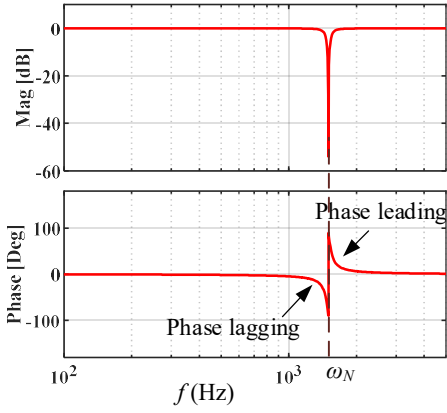Fig. 7. Control diagram of the WT converter with the notch filter
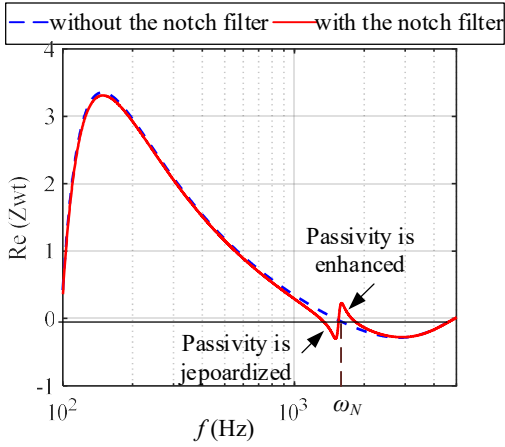
Fig. 8. Bode diagram of the notch filter

Fig. 9. Real part of the output impedance of the WT converter with and without the notch filter.

IV. CASE STUDIES AND SIMULATION RESULTS

To validate the theoretical analysis, time-domain simulations are carried out in the MATLAB/Simulink and PLECS blockset with the nonlinear switching circuit model shown in Fig. 1.

A. Operation of the MMC itself

In this scenario, only the MMC itself is operated to energize cables, transformers, etc, while the wind farms do not operate. As discussed in section II-B, the value of the active resistor adopted in the MMC control has a significant impact on its passivity, i.e., too small R_d will enlarge the non-passive region in the low frequency range while too large R_d will enlarge the non-passive region in the high frequency range, both of which will lead to the risk of unstable operation of the system. This is confirmed by the impedance-based analysis shown in Fig. 10, where Z_{eq} represents the equivalent impedance of the external ac system (including cables, transformers, shunt reactance, etc) connected to the MMC. It is clear that the system cannot be stabilized without active damping (R_d= 0Ω) or with too large active damping (R_d= 300 Ω). As illustrated in Figs. 10 (a) and (c), where the phase difference at the magnitude intersection point is larger than 180°. In contrast, stable operation of the system can be guaranteed with the proper active damping (R_d= 30 Ω), as shown Fig. 10(b).

Fig. 11 shows the corresponding time-domain simulation results with different values of active damping resistor. The unstable operation of the MMC without active damping (R_d= 0Ω) or with too large active damping (R_d= 300 Ω) can be observed in Figs 11 (a) and (c), where the stable operation of the MMC with proper active damping (R_d= 30 Ω) is illustrated in Fig. 11(b). The simulation results shown in Fig. 11 further confirm the passivity based analysis shown in Fig. 4 and impedance-based stability analysis shown in Fig. 10.

(a)

(b)

(c)
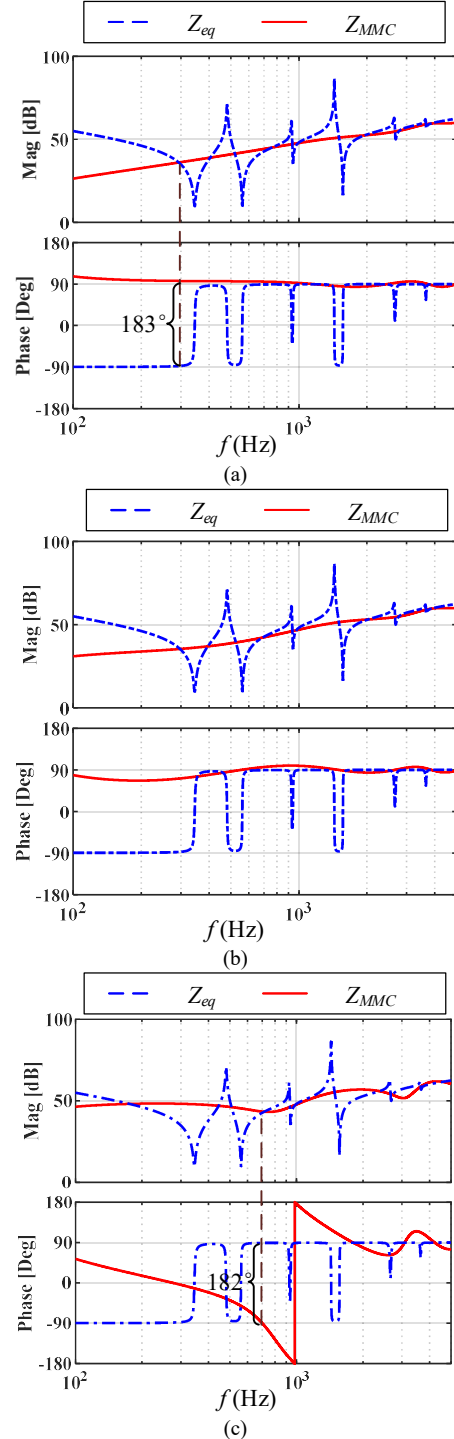
Fig. 10. Output impedance of the MMC and the external AC system. (a)R_d =0 Ω, (b) R_d =30 Ω, (c) R_d =300 Ω
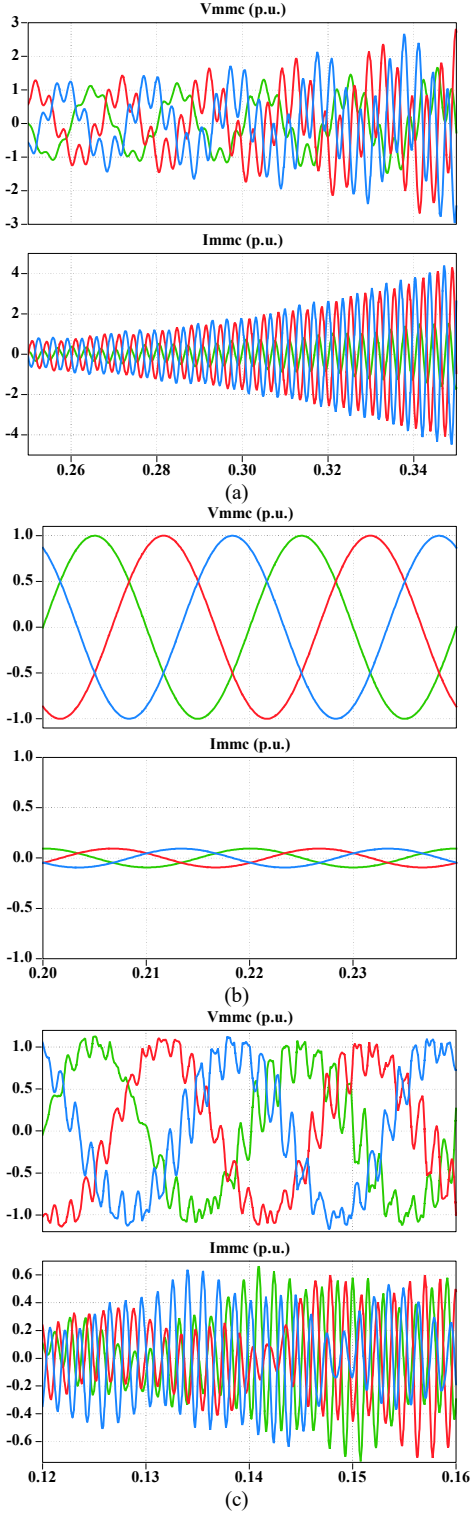
Fig. 11. Time-domain simulation results of the MMC energizes two cables. (a)R_d =0 Ω. (b) R_d =30 Ω. (c) R_d =300 Ω

B. Operation of both MMC and two Wind Farms

In this scenario, both the MMC and two wind farms are operated. Fig. 12 shows the bode diagram of Z_{eq} and Z_{MMC} with different control parameters. As discussed in section II-C, the passivity of the WT converter will be jeopardized by the increased K_{pWT} value, as the unstable case shown in Fig. 12(a).

Although the system can be stabilized by reducing K_{pWT}, as shown in Fig. 12(b), its dynamic performance is also degraded. Therefore, the notch filter is introduced to stabilize the system without reducing the K_{pWT}. The resonance frequency identified in Fig. 12(a) is around 1.65 kHz, and thus the notch filter with ω_N = 1.5 kHz is selected. Fig. 12(c) shows the impedance plot of Z_{eq} and Z_{MMC} with the notch filter, and the stable operation of the system can be observed.
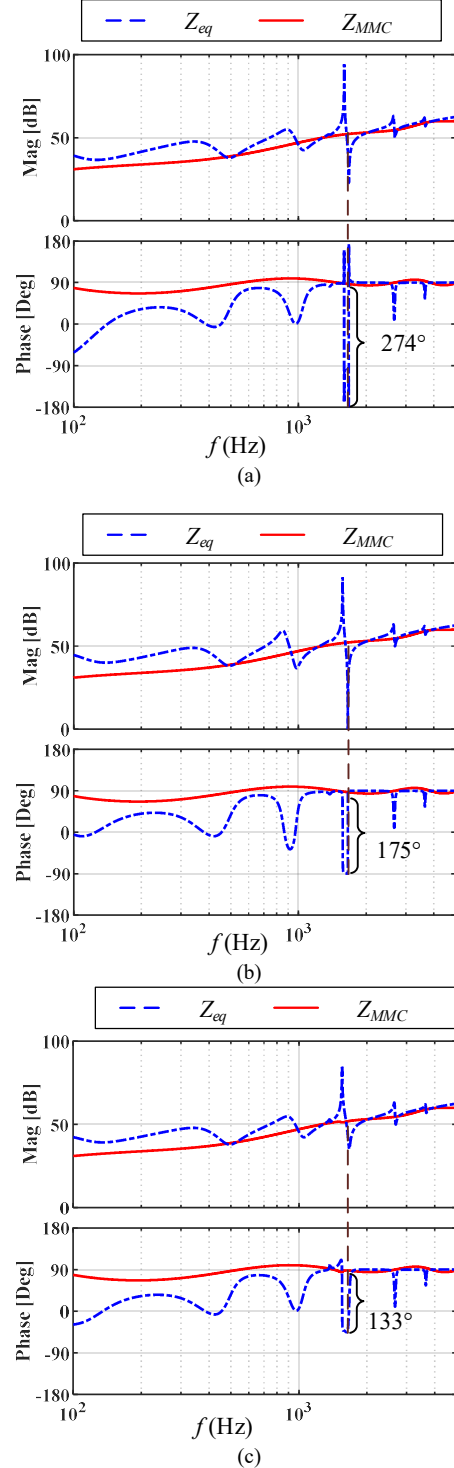

Fig. 12. Output impedance of the MMC and the external AC system. (a) K_{pWT} = 6·10⁻⁷, without notch filter, unstable. (b) K_{pWT} = 2.8·10⁻⁷, without notch filter, stable. (c) K_{pWT} = 6·10⁻⁷, with notch filter, stable.
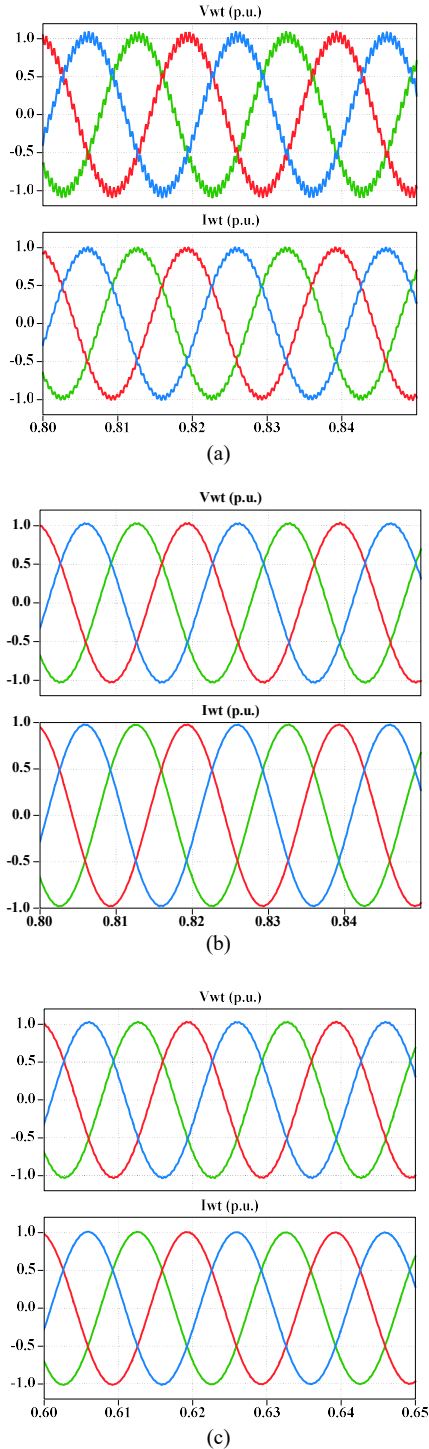
Fig. 13. Time-domain simulation results of the MMC and two wind farms. (a) $K_{PWT} = 6\cdot10^{-7}$, without notch filter, unstable. (b) $K_{PWT} = 2.8\cdot10^{-7}$, without notch filter, stable. (c) $K_{PWT} = 6\cdot10^{-7}$, with notch filter, stable.

Fig. 13 shows the corresponding time-domain simulation results. The unstable operation of the system with $K_{pWT} =6\cdot10^{-7}$ can be observed in Fig 13(a). The system can be stabilized by reducing K_{pWT} to $2.8\cdot10^{-7}$, as shown in Fig. 13(b). Or by adopting a notch filter with $\omega_N = 1.5$ kHz , as shown in Fig. 13(c). The simulation results further confirm the passivity based analysis shown in Fig. 6 and impedance-based stability analysis shown in Fig. 12.

V. CONCLUSION

This paper performs a systematic passivity based stability analysis of an OWF connected to a MMC-HVDC, the main findings are summarized as follows:

1) The active damping used in the MMC control could enhance its passivity in the low-frequency range, but will jeopardize it in the high-frequency range due to the delay effect.
2) Due to the delay effect, the passivity of the MMC and the OWFs are degraded with the increased proportional gain of the controller. Therefore, careful tradeoff between the system stability and dynamic performance is needed during the parameters tuning procedure.
3) The notch filter adopted in the OWF control will jeopardize the system passivity in the frequency range which is lower than its central frequency, but could enhance the passivity in the frequency range higher than the central frequency. Therefore, it is suggested to tune the central frequency of the notch filter to be lower than the network resonance frequency.

All the findings have been verified by time-domain simulations.

VI. REFERENCES

[1] X. Wang and F. Blaabjerg, "Harmonic stability in power electronic based power systems: concept, modeling, and analysis," *IEEE Trans. Smart Grid*, vol. 10, no. 3, pp. 2858–2870, May. 2019.
[2] X. Wang, L. Harnefors, and F. Blaabjerg, "Unified impedance model of grid-connected voltage-source converters," *IEEE Trans. Power Electron., IEEE Trans. Power Electron.*, vol. 33, no. 2, pp. 1775-1787, Feb. 2018.
[3] C. Buchhagen, M. Greve, A. Menze, and J. Jung, "Harmonic stability— Practical experience of a TSO," in *Proc. Wind Integr. Workshop*, Vienna, Austria, Nov. 2016, pp. 1–6.
[4] J. Sun, "Impedance-based stability criterion for grid-connected inverters," *IEEE Trans. Power Electron.*, vol. 26, no. 11, pp. 3075–3078, Nov. 2011.
[5] L. Harnefors, X. Wang, A. Yepes, and F. Blaabjerg, "Passivity-based stability assessment of grid-connected VSCs - an overview," *IEEE Jour. Emer. Select. Top. Power Electron.*, vol. 4, no. 1, pp. 116-125, Mar. 2016.
[6] L. Harnefors, A. G. Yepes, A. Vidal, and J. Doval-Gandoy, "Passivity based controller design of grid-connected VSCs for prevention of electrical resonance instability," *IEEE Trans. Ind. Electron.*, vol. 62, no. 2, pp. 702–710, Feb. 2015
[7] Ł. H. Kocewiak, J. Hjerrild and C. L. Bak, "Wind Turbine Converter Control Interaction with Complex Wind Farm Systems," *IET Renewable Power Generation*, pp. 1-10, 2013.
[8] J. Dannehl, M. Liserre, and F. W. Fuchs, "Filter-based active damping of voltage source converters with *LCL* filter," *IEEE Trans. Ind. Electron.*, vol. 58, no. 8, pp. 3623−3633, Aug. 2011.
[9] R. P. Alzola, M. Liserre, F. Blaabjerg, M. Ordonez, and T. Kerekes, "A self-commissioning notch filter for active damping in a three-phase *LCL*-filter- based grid-tie converter," *IEEE Trans. Power Electron.*, vol. 29, no. 12, pp. 6754−6761, Dec. 2014.
[10] W. Yao, Y. Yang, X. Zhang, F. Blaabjerg, and P. C. Loh, "Design and analysis of robust active damping for *LCL* filters using digital notch filters," *IEEE Trans. Power Electron.*, vol. 32, no. 3, pp. 2360−2375, Mar. 2017.
[11] S. Zhang, S. Jiang, X. Lu, B. Ge, and F. Z. Peng, "Resonance issues and damping techniques for grid connected inverters with long transmission cable," *IEEE Trans. Power Electron.*, vol. 29, no. 1, pp. 110−120, Jan. 2014.
[12] H. Wu, X. Wang, and L. Kocewiak, "Impedance-based stability analysis of voltage-controlled MMCs feeding linear AC systems," *IEEE J. Emerg. Sel. Topics Power Electron.*, early access, 2019.